Crossover from Super- to Subdiffusive Motion and Memory Effects in Crystalline Organic Semiconductors

G. De Filippis,[1] V. Cataudella,[1] A. S. Mishchenko,[2] N. Nagaosa,[2,3] A. Fierro,[4] and A. de Candia[5]
[1]SPIN-CNR and Dipartimento di Fisica, Università di Napoli Federico II, I-80126 Napoli, Italy
[2]RIKEN Center for Emergent Matter Science (CEMS), Wako, Saitama 351-0198, Japan
[3]Department of Applied Physics, The University of Tokyo, 7-3-1 Hongo, Bunkyo-ku, Tokyo 113-8656, Japan
[4]SPIN-CNR Complesso Universitario di Monte S. Angelo, I-80126 Napoli, Italy
[5]INFN, SPIN-CNR, and Dipartimento di Fisica, Università di Napoli Federico II, I-80126 Napoli, Italy
(Received 13 August 2014; published 24 February 2015)

The transport properties at finite temperature of crystalline organic semiconductors are investigated, within the Su-Schrieffer-Heeger model, by combining an exact diagonalization technique, Monte Carlo approaches, and a maximum entropy method. The temperature-dependent mobility data measured in single crystals of rubrene are successfully reproduced: a crossover from super- to subdiffusive motion occurs in the range $150 \leq T \leq 200$ K, where the mean free path becomes of the order of the lattice parameter and strong memory effects start to appear. We provide an effective model, which can successfully explain features of the absorption spectra at low frequencies. The observed response to slowly varying electric field is interpreted by means of a simple model where the interaction between the charge carrier and lattice polarization modes is simulated by a harmonic interaction between a fictitious particle and an electron embedded in a viscous fluid.

DOI: 10.1103/PhysRevLett.114.086601 PACS numbers: 72.80.Le, 71.38.-k, 78.40.Me

Small molecule organic semiconductors, crystals of small molecules held together by van der Waals forces, are the focus of intensive research activity, being the material basis for organic electronics and, in particular, for plastic electronics, a rapidly developing field [1]. Because of the weak van der Waals intermolecular bonding, there is a small overlap between the electronic orbitals of these small molecules leading to narrow electronic bands: the transfer integral t turns out to be about 100 meV [2,3]. At the same time, the electron-phonon interaction (EPI) plays a crucial role [4], and now, it is well established that it stems from Peierls's coupling mechanism [5]. EPI exhibits a strong momentum dependence and, given the pronounced anisotropy of these compounds [6], typically the coupling of the electrons with the lattice vibrations is described by using a one-dimensional tight-binding model involving Einstein phonons with the lattice displacements affecting the electronic hopping integral [2,7] (Su-Schrieffer-Heeger coupling [8]). However, the understanding of charge transport in organic semiconductors remains limited. Indeed, from an experimental point of view, ultrapure crystals of pentacene or rubrene exhibit (1) thermally activated transport at low temperatures [6,9,10] (up to $\simeq$160 K), and (2) a bandlike mobility up to room temperature; i.e., the mobility decreases as $T^{-\gamma}$ with $\gamma \simeq 2$ [9,11]. At the same time, at room temperature, optical absorption spectra are characterized by a broad peak centered around 40 meV [12], reminiscent of disordered systems in the insulating phase. It has been shown that the rapid drop of the mobility below 160 K is due to the crossover to the trap-dominated regime (extrinsic disorder). Measurements of the transverse Hall conductivity [9,13] allowed us to extract the intrinsic, trap-free mobility that always increases with cooling (shallow traps do not contribute to the Hall voltage since the Lorentz force is zero for these charge carriers). It remains to explain the puzzle regarding the simultaneous presence of the signature of intrinsic bandlike transport (power-law dependence of mobility vs temperature) and localized states [absorption spectra feature broad peak centered at finite frequency, whereas in the Drude model the optical conductivity (OC) shows a maximum at $\omega = 0$]. The starting point of several approaches present in the literature is the mechanical softness of these compounds: the characteristic energy of the lattice transverse modes ω_0 is about 5 meV, which is much less than the electronic transfer integral t [3,14]. Then the idea is to use the adiabatic approximation: the phonon variables are treated classically, and the electron contribution to the partition function is calculated at fixed lattice displacements neglecting the retardation effects [15]. In the one-dimensional case, the problem turns out to be equivalent to that of a particle in the presence of an off-diagonal disorder, which provides a vanishing mobility (Anderson localization [16]). In order to overcome this difficulty, the fluctuations of the lattice vibrations, completely neglected in the adiabatic approximation (it becomes exact when $\omega_0 \to 0$ and the ionic mass $M \to \infty$ keeping $k = M\omega_0^2$ *constant* [17]), have to be taken into account. To this aim, it has been proposed (i) to employ mixed quantum-classical simulations based on the Ehrenfest coupled equations [14], (ii) to neglect

vertex corrections in the OC calculation [18], (iii) to introduce an *ad hoc* energy broadening of the system energy levels [15], and (iv): to use the relaxation time approximation [19]. All these approximated approaches either (1) contain external parameters that the theory is not able to fix in a self-consistent way [15,19], or (2) although able to reproduce a power-law dependence of mobility vs temperature [14], do not restore the conductivity values quantitatively [14,18]. It is clear that transport properties crucially depend on the exact dynamics of the lattice at long times. In this Letter, we go beyond the adiabatic approximation: both lattice and electronic degrees of freedom obey exactly (from a numeric point of view) quantum dynamics. We combine exact an diagonalization technique [20], diagrammatic [21] and worldline [22] Monte Carlo approaches, and a maximum entropy method [23] to obtain an unbiased result. The model Hamiltonian is given by (see also the Supplemental Material [24])

$$H = \sum_k (\epsilon_k c_k^\dagger c_k + \omega_0 b_k^\dagger b_k) + \sum_{q,k} (M_{q,k} c_{k+q}^\dagger c_k b_q + \text{H.c.}), \tag{1}$$

where $\epsilon_k = -2t\cos(ka)$ denotes the electron band with hopping t, $c_k^\dagger$ ($b_k^\dagger$) represents the momentum electron (phonon) creation operator, and Einstein optical phonons have frequency ω_0. The EPI vertex is $M_{q,k} = 2i\tilde{\alpha}t/\sqrt{N}(\sin(k+q)a - \sin(ka))$ describing the transfer integral modulation on the distance between nearest neighbors with strength $\tilde{\alpha}$ (N denotes the number of sites and a is the lattice parameter). We use units such that $\hbar = e = k_B = 1$, where e is the electronic charge and k_B is the Boltzmann constant. We shall study the system by assuming values of the parameters typical of single-crystal organic semiconductors, taking rubrene as a case study [7]. We set $a = 7.2$ Å, $\omega_0 = 0.05t$, $\tilde{\alpha} = 0.092$, and $t = 93$ meV.

Within the linear response theory, the light absorption, at low densities, is proportional to the particle concentration. The proportionality constant is OC [31]

$$\sigma(z) = \frac{i}{z}(\Pi(z) - \Gamma), \tag{2}$$

where z lies in the complex upper half-plane, $z = \omega + i\epsilon$ with $\epsilon > 0$; the quantity Γ is

$$\Gamma = -\int_0^\beta ds \langle j(s) j(0) \rangle, \tag{3}$$

and $\Pi(z)$ represents the current-current correlation function

$$\Pi(z) = -i\int_0^\infty d\tau e^{iz\tau} \langle [j(\tau), j(0)] \rangle. \tag{4}$$

In Eq. (4) [Eq. (3)] $j(\tau)$ [$j(s)$] is the real-time (imaginary-time) Heisenberg representation of the current operator

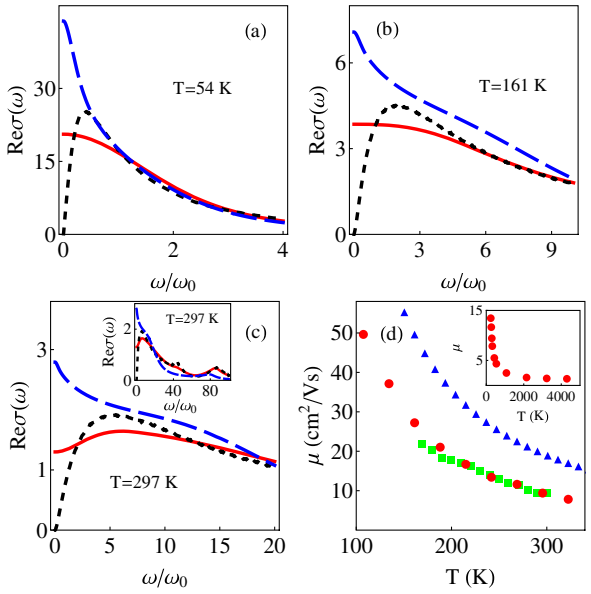

FIG. 1 (color online). [(a)–(c)] OC, in units of $a^2e^2/\hbar$, in different approximations: exact results (solid red line), Boltzmann (long-dashed blue line), and adiabatic (short-dashed black line) approaches. (d) Temperature dependence of the mobility in rubrene [9] (green squares) compared with exact results (red circles) and Boltzmann approach (blue triangles). In the inset is mobility (exact results in units cm^2/Vs) in a wider range of temperatures.

(see the Supplemental Material [24]) and $[,]$ denotes the commutator, $\langle\rangle$ indicates the thermal average, and $\beta = 1/T$. The real part of the OC [$\text{Re}\sigma(\omega) = \text{Re}\sigma(\omega + i\epsilon)$, $\epsilon \to 0^+$] is related to the imaginary-time current-current correlation function

$$\Pi(s) = \int_{-\infty}^{\infty} d\omega \frac{1}{\pi} \frac{\omega e^{-\omega s}}{1 - e^{\beta\omega}} \text{Re}\sigma(\omega). \tag{5}$$

The function $\Pi(s)$ has been calculated by using diagrammatic [21] and worldline [22] Monte Carlo methods, checking that both approaches give the same results. The dynamical spectra, then, is extracted from the integral equation, Eq. (5), through the maximum entropy method [23]. In particular, we used the Bryan's method choosing, as default model, the OC obtained through exact diagonalization on a lattice of 20 sites with periodic boundary conditions (at the investigated temperatures the mean free path, MFP, is less than $6a$ so that such a small lattice provides a very good starting point).

In Fig. 1 we plot the OC at three different temperatures, comparing exact results obtained from the numerical simulations with those of two limiting cases stemming from Boltzmann [32] and adiabatic approaches [15]. It is evident that neither Boltzmann treatment, involving one-phonon scattering processes, nor the adiabatic approach, where electrons move in a static lattice and the mobility goes to zero at any temperature, are able to correctly describe the

charge carrier dynamics at low frequencies [33]. Indeed, only at very short times ($\omega \gg \omega_0$) is the OC behavior well captured by the adiabatic treatment [see the inset of Fig. 1(c)]: at high frequencies the Franck-Condon principle can be invoked, and the lattice is frozen during electron transitions between different energetic levels. On the other hand, at long times ($\omega \leq \omega_0$) the lattice dynamic cannot be neglected, and the OC can be obtained only by treating correctly both electron and lattice vibration fluctuations. In Fig. 1(d) the temperature-dependent mobility data measured in single crystals of rubrene [9] (intrinsic, trap-free mobility) are successfully compared with our numerical results $\mu = \mathrm{Re}\sigma(\omega \to 0^+)/e$; our approach is able to recover both qualitatively and quantitatively the features of the absorption spectra at low frequencies. We emphasize [see inset of Fig. 1(d)] the interesting mobility behavior at very high (but unphysical) temperatures indicating the saturation of the direct current conductivity at $T \simeq 1000$ K.

Also worthy of note is the remarkable behavior of the resistivity $\rho(\omega) = 1/\sigma(\omega)$, as function of the frequency, shown in Fig. 2(a) at different temperatures. At $T = 54$ K there is a single absolute minimum at $\omega = 0$, at $T = 161$ K the curve is flat at this minimum, and finally at $T = 297$ K two minima develop at finite frequency. In order to investigate more deeply the microscopic physical mechanisms underlying this finding, we have calculated the instantaneous diffusivity [34]

$$D(\tau) = \frac{1}{2}\frac{d\Delta x^2}{d\tau} = \int_0^\infty d\omega \frac{\mathrm{Re}\sigma(\omega)\sin(\omega\tau)}{\pi \tanh(\frac{\beta\omega}{2})}, \qquad (6)$$

and the quantity $\Delta x^2 = \langle (x(\tau) - x(0))^2 \rangle$, i.e., the mean-square displacement (MSD) of the position operator x. Locally, around τ_0, MSD grows as $\tau^{\alpha(\tau_0)}$ with the diffusion exponent $\alpha(\tau_0)$ equal to the logarithmic slope of Δx^2: $\alpha(\tau_0) = \tau_0 D(\tau_0)/\mathrm{MSD}(\tau_0)$. In Fig. 2(b) we plot the diffusion exponent vs the time τ (in units of $1/\omega_0$) at different temperatures. At very short times $\alpha(\tau)$ is about 2; i.e., the motion is ballistic independently on the temperature. However, after a transient time the curves differ significantly. Indeed, at $T = \omega_0 = 54$ K the evolution is always superdiffusive [$\alpha(\tau) > 1$] and approaches, only at long times, diffusive behavior $\alpha(\tau) \to 1$. On the other hand, at $T = 5.5\omega_0 = 297$ K, there is a broad range of values of τ for which $\alpha(\tau) < 1$, signaling the onset of subdiffusive motion. However, also here, at very large times $\tau \gg 1/\omega_0$, the motion becomes diffusive. Finally, in the range $150 \leq T \leq 200$ K [see also inset of Fig. 2(b)] the ballistic motion is rapidly followed by the diffusion. Further insight into the problem is provided by the analysis of the optical relaxation time and the MFP. To this aim, the OC is written in terms of the memory function $M(\omega)$ [35],

$$\sigma(\omega) = -i\frac{\Gamma}{\omega + iM(\omega)}. \qquad (7)$$

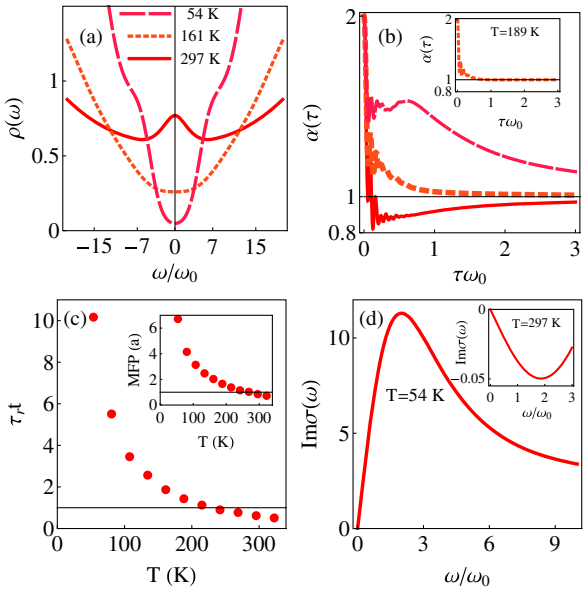

FIG. 2 (color online). Resistivity (a) and diffusion exponent (b) at different temperatures (symbols are the same in the two panels). (c) τ_r (in units of $1/t$) vs temperature (in the inset MFP in units of a). (d) Imaginary part of the conductivity at two temperatures.

At $\omega = 0$ the function M is real and determines the reciprocal of the optical relaxation time $1/\tau_r$ so that the mobility turns out to be $\mu = -\tau_r\Gamma$. This last relation allows us to extract τ_r [in SSH model the quantity Γ is equal to the sum of thermal averages of the first and third term of the Hamiltonian Eq. (1)]. The MFP is defined by $\mathrm{MFP} = v\tau_r$, and a rough estimate of the average velocity v can be obtained by $v \simeq \sqrt{\Pi(\tau = 0)}$. In Fig. 2(c) [inset of Fig. 2(c)] we plot the temperature dependence of τ_r (MFP). By increasing T, τ_r (MFP) decreases and becomes of the order of $1/t$ (the lattice parameter) just around 200 K. The crossover from super-to subdiffusive motion then signals the onset of the incoherent motion regime, where the charge carriers are strongly scattered in the real space and the bandlike picture breaks down. Interestingly the imaginary part of the conductivity, at low frequencies, changes sign across the crossover [see Fig. 2(d)] becoming negative when $T > 200$ K.

It is possible to show that the subdiffusion is a direct consequence of the memory effects. To this aim, we note that the Mori formalism allows us to reformulate, in an exact way, the Heisenberg equation of motion of any dynamical variable in terms of a generalized Langevin equation [36]. It is possible by introducing a Hilbert space of operators (whose invariant parts are set to be zero) where the inner product is defined by

$$(A, B) = \frac{1}{\beta}\int_0^\beta \langle e^{sH} A^\dagger e^{-sH} B\rangle ds. \qquad (8)$$

In particular, the current operator obeys the equation

$$\frac{dj}{d\tau} = -\int_0^\tau M(\tau - r) j(r) dr + f(\tau), \qquad (9)$$

where the quantity $f(\tau)$ represents the "random force," that is, at any time, orthogonal to j and is related to the memory function M by the fluctuation-dissipation formula. The solution of this equation can be expressed as $j(\tau) = \Sigma(\tau) j + \tilde{j}(\tau)$, i.e., $\Sigma(\tau) = (j, j(\tau))/(j, j)$ describes the time evolution of the projection of $j(\tau)$ on the axis parallel to j and represents the relaxation of the current operator (it is related to the Fourier transform of the real part of OC), whereas $\tilde{j}(\tau)$ is always orthogonal to j. In Figs. 3(a) and 3(b) we compare $\mathrm{Re}\Sigma(\tau)$ and the memory function $M(\tau)$ at $T = 54$ K and $T = 297$ K. The plots point out that while at low T the relaxation occurs on a time scale very much longer than the one characteristic of the memory function, at high T, where subdiffusion sets in, the two time scales are of the same order. It is a clear indication of the presence of strong memory effects (breakdown of the Markovian approximation) that arise at $T > 200$ K.

Particularly interesting is the time response of the polarization operator P [37]. It obeys an equation similar to Eq. (9). We indicate with $R(\tau)$ the function $(P, P(\tau))$ that is related to the relaxation function of P and with $\chi(\tau)$ the dielectric susceptibility [it is obtained by replacing $j(\tau)$ with $P(\tau)$ in Eq. (4) and removing the minus sign] that provides the response of P to a weak external field. It is possible to show that $dR/d\tau = -(1/\beta)\chi(\tau)$ and $\chi(z) = i\sigma(z)/z$ so that the knowledge of $\sigma(z)$ fully determines the system response. In particular, if we assume a Drude model for the charge carriers, i.e., $\sigma(z) = (\sigma_{dc}/\tilde{\tau}_r)[i/(z + i/\tilde{\tau}_r)]$ [$\sigma_{dc} = \mathrm{Re}\sigma(\omega = 0)$], $R(\tau)$ turns out to be $\Delta R(\tau) = R(\tau) - R(\tau = 0) = -T\sigma_{dc}[\tau + \tilde{\tau}_r(e^{-\tau/\tilde{\tau}_r} - 1)]$. In Fig. 3(c) we plot $G(\tau) = \Delta R(\tau) + T\sigma_{dc}\tau$ vs τ at different temperatures. At $T = 57$ K, $G(\tau)$ is very close to the function $T\sigma_{dc}\tau_r(1 - e^{-\tau/\tau_r})$; i.e., the Drude model with $\tilde{\tau}_r = \tau_r$ (best fit recovers just $\tilde{\tau}_r = \tau_r$) reproduces very well the behavior of P relaxation at almost any time. By increasing temperature it is evident, from the plots in Fig. 3(b), that a Drude-like behavior is limited to a smaller range of τ values and a negative contribution appears, whose relaxation occurs on a longer time scale. We found that a linear superposition of Drude- and Drude-Lorentz-like (damped harmonically bound particles, see the Supplemental Material [24]) contributions represents a good fit of the function $G(\tau)$ at any temperature [see for example the inset of Fig. 3(c)]. In any case it is worthy of note that the best fit recovers $\tilde{\tau}_r = \tau_r$ at any temperature. While in the Drude model the memory effects are absent [$M(\tau) \propto \delta(\tau)$], in the Drude-Lorentz model the memory function is a superposition of two contributions: the first one is again $\propto \delta(\tau)$, whereas the other one is constant as function of the time τ. As a direct consequence of Eq. (7), the mobility in Drude-Lorentz model is zero and the maximum of OC is located at finite frequency. This explains the simultaneous presence of the signature of localized states (Drude-Lorentz model) and

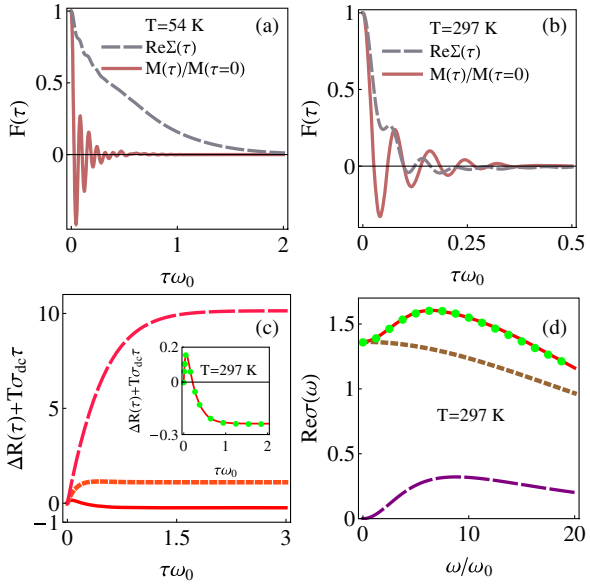

FIG. 3 (color online). [(a) and (b)] Comparison between current operator relaxation function and memory function at two temperatures; $F(\tau)$ stands for the dimensionless quantities $\mathrm{Re}\Sigma(\tau)$ and $M(\tau)/M(\tau = 0)$. (c) Relaxation function of the polarization [symbols as in panel of Fig. 2(a)] at different temperatures; in the inset is a comparison with the model (green circles). (d) $\mathrm{Re}\sigma(\omega)$: exact results (red solid line); Drude-Lorentz contribution (DLC) (long-dashed purple line), and note that the mobility of DLC is zero; Drude contribution (DC) (short-dashed brown line); DCL + DC (green circles).

intrinsic bandlike transport (stemming from the Drude term). Indeed, Fig. 3(d) shows that the linear superposition of two (Drude- and Drude-Lorentz-like) contributions, with parameters fixed by the best-fit procedure for $G(\tau)$, is able to successfully describe the OC low frequencies behavior. Here, the response can be described by simulating the interaction between the charge carrier and lattice polarization modes by a harmonic interaction between a fictitious particle and an electron embedded in a viscous fluid. The center of mass (relative) motion turns out to be well represented by a Drude-like (Drude-Lorentz-like) model (see the Supplemental Material [24]). It is worthy of note that the dynamics of the relative motion of this effective system is underdamped below 200 K and becomes overdamped above 200 K. We found that the Drude-Lorenz-like contribution turns to be out negligible at $T < 150$ K. On the other hand, above 150 K, by increasing T the weight of the Drude-Lorentz-like contribution grows: this explains the change of sign of $\mathrm{Im}\sigma(\omega)$ at low frequencies observed in Fig. 2(d). Indeed, $\mathrm{Im}\sigma(\omega)$ describes the current transport out of phase with the external field. $\mathrm{Im}\sigma(\omega) > 0$ [$\mathrm{Im}\sigma(\omega) < 0$] in the Drude (Drude-Lorentz) model: at $T = 200$ K there is a crossover from inductive behavior, due to the inertia of electrons, to capacitive behavior, due to the relative motion of an electron-fictitious particle system.

In conclusion, by combining an exact diagonalization technique, Monte Carlo approaches, and a maximum

entropy method, we found that a crossover from super- to subdiffusive motion occurs in the range $150 \leq T \leq 200$ K, where the relaxation time τ_r is of the order of $1/t$ ($\tau_r \ll 1/\omega_0$), the motion becomes incoherent, and strong memory effects start to appear. OC low frequencies features are well described by an effective model where the electron and a fictitious particle, embedded in a viscous fluid, harmonically interact with each other.

N. N. is supported by Grant-in-Aids for Scientific Research (S) (No. 24224009) from the Ministry of Education, Culture, Sports, Science and Technology (MEXT) of Japan and Strategic International Cooperative Program (Joint Research Type) from the Japan Science and Technology Agency.

[1] J. M. Shaw and P. F. Seidler, IBM J. Res. Dev. **45**, 3 (2001); H. Hoppe and N. S. Sariciftci, J. Mater. Res. **19**, 1924 (2004); H. E. Katz, Chem. Mater. **16**, 4748 (2004); S. R. Forrest, Nature (London) **428**, 911 (2004); M. E. Gershenson, V. Podzorov, and A. F. Morpurgo, Rev. Mod. Phys. **78**, 973 (2006).

[2] A. Troisi and G. Orlandi, J. Phys. Chem. B **109**, 1849 (2005).

[3] V. Coropceanu, J. Cornil, D. A. da Silva Filho, Y. Olivier, R. Silbey, and J. L. Bredas, Chem. Rev. **107**, 926 (2007).

[4] V. M. Kenkre, J. D. Andersen, D. H. Dunlap, and C. B. Duke, Phys. Rev. Lett. **62**, 1165 (1989); K. Hannewald and P. A. Bobbert, Appl. Phys. Lett. **85**, 1535 (2004).

[5] M. Zoli, Phys. Rev. B **66**, 012303 (2002); V. M. Stojanovic and M. Vanevic, *ibid.* **78**, 214301 (2008); Y. Li, Y. Yi, V. Coropceanu, and J. L. Bredas, *ibid.* **85**, 245201 (2012).

[6] V. Podzorov, E. Menard, A. Borissov, V. Kiryukhin, J. A. Rogers, and M. E. Gershenson, Phys. Rev. Lett. **93**, 086602 (2004).

[7] A. Troisi, Adv. Mater. **19**, 2000 (2007).

[8] W. P. Su, J. R. Schrieffer, and A. J. Heeger, Phys. Rev. Lett. **42**, 1698 (1979); D. J. J. Marchand, G. De Filippis, V. Cataudella, M. Berciu, N. Nagaosa, N. V. Prokofev, A. S. Mishchenko, and P. C. E. Stamp, Phys. Rev. Lett. **105**, 266605 (2010).

[9] V. Podzorov, E. Menard, J. A. Rogers, and M. E. Gershenson, Phys. Rev. Lett. **95**, 226601 (2005).

[10] N. A. Minder, S. Ono, Z. Chen, A. Facchetti, and A. F. Morpurgo, Adv. Mater. **24**, 503 (2012).

[11] O. D. Jurchescu, J. Baas, and T. T. M. Palstra, Appl. Phys. Lett. **84**, 3061 (2004); V. C. Sundar, J. Zaumseil, V. Podzorov, E. Menard, R. L. Willet, T. Someya, M. E. Gershenson, and J. A. Rogers, Science **303**, 1644 (2004); I. N. Hulea, S. Fratini, H. Xie, C. L. Mulder, N. N. Iossad, G. Rastelli, S. Ciuchi, and A. F. Morpurgo, Nat. Mater. **5**, 982 (2006).

[12] Z. Q. Li, V. Podzorov, N. Sai, M. C. Martin, M. E. Gershenson, M. Di Ventra, and D. N. Basov, Phys. Rev. Lett. **99**, 016403 (2007).

[13] J. Takeya, K. Tsukagoshi, Y. Aoyagi, T. Takenobu, and Y. Iwasa, Jpn. J. Appl. Phys., Part 2 **44**, L1393 (2005).

[14] A. Troisi and G. Orlandi, Phys. Rev. Lett. **96**, 086601 (2006).

[15] V. Cataudella, G. De Filippis, and C. A. Perroni, Phys. Rev. B **83**, 165203 (2011).

[16] P. W. Anderson, Phys. Rev. **109**, 1492 (1958).

[17] G. De Filippis, V. Cataudella, S. Fratini, and S. Ciuchi, Phys. Rev. B **82**, 205306 (2010).

[18] S. Fratini and S. Ciuchi, Phys. Rev. Lett. **103**, 266601 (2009); S. Ciuchi and S. Fratini, Phys. Rev. B **86**, 245201 (2012).

[19] S. Ciuchi, S. Fratini, and D. Mayou, Phys. Rev. B **83**, 081202(R) (2011).

[20] G. De Filippis, V. Cataudella, A. S. Mishchenko, and N. Nagaosa, Phys. Rev. B **85**, 094302 (2012); F. Novelli, G. De Filippis, V. Cataudella, M. Esposito, F. Cilento, E. Sindici, A. Amaricci, C. Giannetti, D. Prabhakaran, S. Wall, A. Perucchi, S. Dal Conte, G. Cerullo, M. Capone, A. Mishchenko, N. Nagaosa, F. Parmigiani, and D. Fausti, Nat. Commun. **5**, 5112 (2014).

[21] N. V. Prokof'ev and B. V. Svistunov, Phys. Rev. Lett. **81**, 2514 (1998); A. S. Mishchenko, N. V. Prokof'ev, A. Sakamoto, and B. V. Svistunov, Phys. Rev. B **62**, 6317 (2000); A. S. Mishchenko, N. Nagaosa, Z.-X. Shen, G. De Filippis, V. Cataudella, T. P. Devereaux, C. Bernhard, K. W. Kim, and J. Zaanen, Phys. Rev. Lett. **100**, 166401 (2008).

[22] A. de Candia, V. Cataudella, G. De Filippis, A. S. Mishchenko, and N. Nagaosa (to be published).

[23] M. Jarrell and J. E. Gubernatis, Phys. Rep. **269**, 133 (1996).

[24] See the Supplemental Material at http://link.aps.org/supplemental/10.1103/PhysRevLett.114.086601 for (i) a discussion on the Hamiltonian, the lowest electronic band, the optical conductivity and the spectral weight function at $T = 0$ K; (ii) a brief introduction to the Drude-Lorentz model and the Feynman polaron model, which includes Refs. [25–30].

[25] F. Ortmann, F. Bechstedt, and K. Hannewald, Phys. Status Solidi B **248**, 511 (2011).

[26] V. Cataudella, G. De Filippis, and G. Iadonisi, Phys. Rev. B **60**, 15163 (1999).

[27] S. Engelsberg and J. R. Schrieffer, Phys. Rev. **131**, 993 (1963).

[28] G. D. Mahan, *Many Particle Physics* (Plenum, New York, 1981).

[29] R. P. Feynman, Phys. Rev. **97**, 660 (1955).

[30] G. De Filippis, V. Cataudella, A. S. Mishchenko, C. A. Perroni, and J. T. Devreese, Phys. Rev. Lett. **96**, 136405 (2006).

[31] S. Mukerjee and B. S. Shastry, Phys. Rev. B **77**, 245131 (2008).

[32] G. De Filippis, V. Cataudella, A. de Candia, A. S. Mishchenko, and N. Nagaosa, Phys. Rev. B **90**, 014310 (2014).

[33] Boltzmann treatment provides results: (i) quantitatively different (from the exact data) by a factor of the order of 2 and (ii) exhibiting, in the most interesting range of temperatures, $200 < T < 300$ K, a power-law behavior $\mu \simeq T^{-\gamma}$; however, the index γ turns out to be $\simeq 1.5$, whereas both experimental and theoretical data are characterized by $\gamma \simeq 2$.

[34] R. Kubo, J. Phys. Soc. Jpn. **12**, 570 (1957); D. Mayou, Phys. Rev. Lett. **85**, 1290 (2000); G. Trambly de Laissardiere, J.-P. Julien, and D. Mayou, *ibid.* **97**, 026601 (2006).

[35] W. Götze and P. Wölfle, Phys. Rev. B **6**, 1226 (1972).

[36] H. Mori, Prog. Theor. Phys. **33**, 423 (1965).

[37] Y. Feldman, A. Puzenko, and Y. Ryabov, Chem. Phys. **284**, 139 (2002).